

Nonreciprocal transport in the superconducting state of the chiral crystal $NbGe_2$

Yonglai Liu, Xitong Xu, Miao He, Haitian Zhao, Qingqi Zeng, Xingyu Yang, Youming Zou, Haifeng Du, and Zhe Qu

Citation: Chin. Phys. B, 2024, 33 (**5**): 057402. DOI: 10.1088/1674-1056/ad334b
Journal homepage: http://cpb.iphy.ac.cn; http://iopscience.iop.org/cpb

What follows is a list of articles you may be interested in

Structure and superconducting properties of $Ru_{1-x}Mo_x$ (x = 0.1—0.9) alloys

Yang Fu(付阳), Chunsheng Gong(龚春生), Zhijun Tu(涂志俊), Shangjie Tian(田尚杰), Shouguo Wang(王守国), and Hechang Lei(雷和畅)
Chin. Phys. B, 2024, 33 (**4**): 047404. DOI: 10.1088/1674-1056/ad2a73

Majorana tunneling in a one-dimensional wire with non-Hermitian double quantum dots

Peng-Bin Niu(牛鹏斌) and Hong-Gang Luo(罗洪刚)
Chin. Phys. B, 2024, 33 (**1**): 017403. DOI: 10.1088/1674-1056/ad0145

Distinct behavior of electronic structure under uniaxial strain in $BaFe_2As_2$

Jiajun Li(李佳俊), Giao Ngoc Phan, Xingyu Wang(王兴玉), Fazhi Yang(杨发枝), Quanxin Hu(胡全欣), Ke Jia(贾可), Jin Zhao(赵金), Wenyao Liu(刘文尧), Renjie Zhang(张任杰), Youguo Shi(石友国), Shiliang Li(李世亮), Tian Qian(钱天), and Hong Ding(丁洪)
Chin. Phys. B, 2024, 33 (**1**): 017401. DOI: 10.1088/1674-1056/acd8af

A ten-fold coordinated high-pressure structure in hafnium dihydrogen with increasing superconducting transition temperature induced by enhancive pressure

Yan-Qi Wang(王妍琪), Chuan-Zhao Zhang(张传钊), Jin-Quan Zhang(张金权), Song Li(李松), Meng Ju(巨濛), Wei-Guo Sun(孙伟国), Xi-Long Dou(豆喜龙), and Yuan-Yuan Jin(金园园)
Chin. Phys. B, 2023, 32 (**9**): 097402. DOI: 10.1088/1674-1056/acc934

Anisotropic superconducting properties of $FeSe_{0.5}Te_{0.5}$ single crystals

Jia-Ming Zhao(赵佳铭) and Zhi-He Wang(王智河)
Chin. Phys. B, 2022, 31 (**9**): 097402. DOI: 10.1088/1674-1056/ac5610

RAPID COMMUNICATION

Nonreciprocal transport in the superconducting state of the chiral crystal $NbGe_2$

Yonglai Liu(刘永来)[1,2], Xitong Xu(许锡童)[1,†], Miao He(何苗)[1,2], Haitian Zhao(赵海天)[1,2], Qingqi Zeng(曾庆祺)[1], Xingyu Yang(杨星宇)[1,2], Youming Zou(邹优鸣)[1], Haifeng Du(杜海峰)[1,2], and Zhe Qu(屈哲)[1,2,‡]

[1] *Anhui Key Laboratory of Low-Energy Quantum Materials and Devices, CAS Key Laboratory of Photovoltaic and Energy Conservation Materials, High Magnetic Field Laboratory of Chinese Academy of Sciences (CHMFL), HFIPS, CAS, Hefei* 230031, *China*

[2] *Science Island Branch of Graduate School, University of Science and Technology of China, Hefei* 230026, *China*

(Received 31 January 2024; revised manuscript received 8 March 2024; accepted manuscript online 13 March 2024)

Due to the lack of inversion, mirror or other roto-inversion symmetries, chiral crystals possess a well-defined handedness which, when combined with time-reversal symmetry breaking from the application of magnetic fields, can give rise to directional dichroism of the electrical transport phenomena via the magnetochiral anisotropy. In this study, we investigate the nonreciprocal magneto-transport in microdevices of $NbGe_2$, a superconductor with structural chirality. A giant nonreciprocal signal from vortex motions is observed during the superconducting transition, with the ratio of nonreciprocal resistance to the normal resistance γ reaching 6×10^5 $T^{-1}\cdot A^{-1}$. Interestingly, the intensity can be adjusted and even sign-reversed by varying the current, the temperature, and the crystalline orientation. Our findings illustrate intricate vortex dynamics and offer ways of manipulation on the rectification effect in superconductors with structural chirality.

Keywords: chiral crystals, magnetochiral anisotropy, superconducting vortex, nonreciprocal transport

PACS: 74.25.F–, 74.25.Wx, 73.23.–b **DOI:** 10.1088/1674-1056/ad334b

1. Introduction

The concept of chirality, which refers to situations where all mirror symmetries are broken in an object, plays a vital role in the symmetry properties of nature at all length scales from elementary particles to biological systems.[1] In condensed matter physics, the structural chirality can serve as a guiding principle to find topological materials, guaranteeing the Kramers–Weyl fermions as a universal topological electronic property in all nonmagnetic chiral crystals.[2,3] Moreover, as electrons, spins and phonons distribute themselves along the chiral framework of atomic configurations, their rotational and translational motions couple to give specific physical processes.[4–8] These phenomena include the magnetochiral dichroism exhibited in chiral optical crystals,[9] magnetic skyrmions supported by chiral magnets,[10] nonlocal and nonreciprocal electric transports in chiral metals or semiconductors,[11,12] and possible unconventional superconductivity in superconductors.[13]

The electrical magnetochiral effect, firstly suggested by Rikken *et al.*,[11] is one such nonreciprocal transport effect. It is characterized by the directional I–V characteristics

$$V(B,I) = IR_0(1+\gamma BI), \tag{1}$$

where the coefficient γ describes the ratio of nonreciprocal resistance to the normal resistance, being nonzero only for the chiral or polar lattice symmetry.[4] This phenomenon has been demonstrated in some noncentrosymmetric semimetals and semiconductors like the polar semiconductor BiTeBr, topological insulators $MnBi_2Te_4$ and $ZrTe_5$.[14–18] In superconductors, the nonreciprocal response can be significantly elevated by orders of magnitude compared to non-superconducting systems, owing to the substantial energy scale disparity between the Fermi energy and the superconducting energy gap.[8,19,20] In the noncentrosymmetric superconductors, two types of nonreciprocal charge transport mechanisms have been proposed:[8] below the mean-field transition temperature T_c, the nonreciprocal resistivity is determined from the dynamics of vortices; above T_c, the fluctuation of the superconducting order parameter causes the excess paraconductivity, the extension of which gives the nonlinear response. However, the nonreciprocal superconducting transport has been discovered so far only in a few two-dimensional systems including MoS_2, $SrTiO_3$, $NbSe_2$, etc.,[21–24] and the quasi-two-dimensional system $PbTaSe_2$.[25] Relevant experiments on three-dimensional superconductor with a chiral structure have been lacking, and the identification and classification of the detailed mechanism are still ongoing.[8,25,26]

In this work, we investigate $NbGe_2$, a superconductor possessing a chiral structure. This material has been predicted to be a Kramers–Weyl semimetal, and there have been intense studies on the superconductivity and the fermiology.[27–30] We study in detail the nonreciprocal magneto-transport in microdevices of $NbGe_2$, and report two important results. Firstly, a giant nonreciprocal signal from vortex motions is observed

†Corresponding author. E-mail: xuxitong@hmfl.ac.cn
‡Corresponding author. E-mail: zhequ@hmfl.ac.cn

© 2024 Chinese Physical Society and IOP Publishing Ltd

in the superconducting transition region, with the nonreciprocal ratio γ reaching 6×10^5 $\mathrm{T^{-1}\cdot A^{-1}}$, which is among the largest values ever reported. Secondly, γ can be easily tuned and even sign-reversed by changing parameters including the current, the temperature and the crystalline orientation. These findings demonstrate intricate vortex dynamics in $NbGe_2$ and pave paths of controlling the rectification effect in possible superconducting devices.

2. Method

Single crystals of $NbGe_2$ were synthesized by a chemical vapor transport method using iodine as the transport agent.[30] Prior to the growth, Nb and Ge pieces were firstly arc-melted using an arc furnace under the argon atmosphere to yield the polycrystalline samples of $NbGe_2$. The polycrystals were then crushed and grounded into powers, and further sealed in a quartz tube with 100 mg iodine as the transport agent. The sealed quartz ampoule was placed in a furnace with a temperature gradient of 1000 °C/850 °C and maintained for 7 days. Typical size of the as-grown crystals is around 1 mm in length. Thin plates of the crystal within the crystalline *ab* plane or along the *c* direction were cut out from single crystals using the FEI Helios NanoLab FIB. The lamellas were subsequently transferred to a silicon substrate with pre-deposited gold electrodes and patterned into standard Hall bars. Electrical contacts were made by FIB assisted platinum deposition. A scanning electron microscope image of a $NbGe_2$ microdevice is shown in Fig. 1(b) inset, with typical sample size around $8\times0.8\times0.8$ μm^3. Electrical transport properties were measured in the 12 T C-mag Teslatron PT system. The complex resistance was measured with the SynkTek multichannel lock-in at a driving frequency of 137 Hz. For an ac current $I = I_0 \sin \omega t$, equation (1) gives

$$V = I_0 R_0 \sin \omega t + \frac{1}{2}\gamma I_0^2 R_0 B \left[1 + \sin\left(2\omega t - \frac{\pi}{2}\right)\right]. \quad (2)$$

The in-phase component of the ac voltage at the frequency ω comes from the normal resistance, while the out-of-phase component at the frequency 2ω is read as the second harmonic voltage and[11,31,32]

$$R_{xx}^{2\omega} \overset{\text{def}}{=} \frac{1}{2}\gamma I_0 R_0 B. \quad (3)$$

Symmetrization and anti-symmetrization with respect to magnetic field have been performed to separate the field odd and even components.

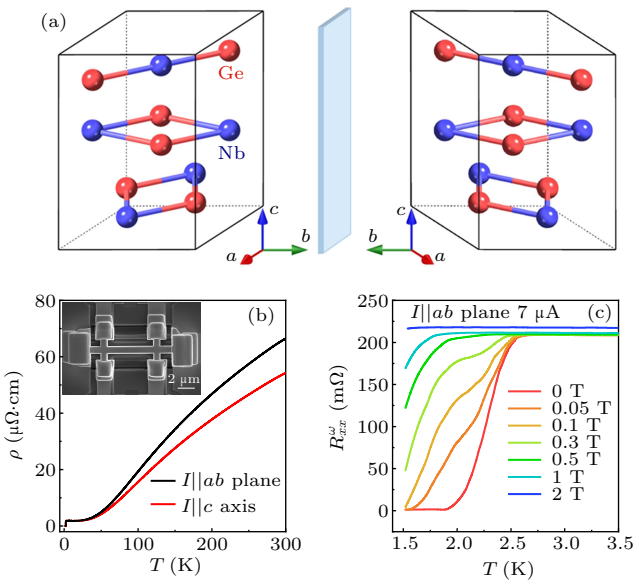


Fig. 1. (a) The chiral crystal structure of $NbGe_2$. (b) Temperature dependence of the resistance (R_{xx}^{ω})of micro-patterned $NbGe_2$ samples measured with $I \parallel ab$ plane (black) and $I \parallel c$ axis (red), both showing a superconducting transition at T_c around 2.25 K. Typical sample size is around $8\times0.8\times0.8$ μm^3. Inset shows schematic illustration of the transport measurement configuration. The scale bar is 2 μm. (c) Temperature dependence of R_{xx}^{ω} at selected magnetic fields for $I \parallel ab$ plane.

3. Results and discussion

$NbGe_2$ belongs to the C40-type transition metal ditetrelides family TX_2 (T = V, Cr, Nb, Ta; and X = Si, Ge). As shown in Fig. 1(a), it possesses a hexagonal structure of the space group $P6_222$ (No. 180).[28] Each unit cell consists of three layers of $NbGe_2$, with the middle and the bottom slices shift along the *b* and *a* axes for half a period, respectively. Such an alternative displacement gives rise to a typical chiral structure which cannot overlap itself under the mirror reflection. We have performed basic electrical transport measurements on our microdevices for both the $I \parallel ab$ plane and $I \parallel c$ axis configurations. The overall anisotropy is relatively weak. At room temperature, the resistivity ρ_{xx}(300 K) is 66 μΩ·cm for $I \parallel ab$ plane, and 54 μΩ·cm for $I \parallel c$ configuration. The temperature dependence of the resistance shows typical metallic behaviors (Fig. 1(b)), and the superconducting transition occurs at $T_c = 2.25$ K, slightly higher than previous reports in millimeter-sized samples,[33] which may be due to the Ga-inclusion during the FIB milling. With the application of an out-of-plane magnetic field, the superconducting transition is broadened as shown in Fig. 1(c). The critical magnetic field at $T = 1.6$ K is approximately 0.5 T as obtained from the half value of the resistance in the normal state, which is also larger than previous results.[28]

We now focus on the magnetic field dependence of the first (R_{xx}^{ω}) and the second ($R_{xx}^{2\omega}$) harmonic resistances, as depicted in Fig. 2. Two experimental configurations are concerned. For the first device, 7 μA electric current is flowing along the crystalline *a* axis and the magnetic field is along the crystalline *c* axis, while for the second, the current is along the *c* axis and the field along the *a* axis. As shown in Figs. 2(a) and 2(d), the first harmonic resistance R_{xx}^{ω} is zero at low field, and gradually approaches the normal state resistance under the application of the magnetic field. The overall profile is

symmetric with respect to the field, which is common in ordinary superconductors. The second harmonic resistance $R_{xx}^{2\omega}$, on the contrary, exhibits a prominent antisymmetric behavior. For the $I \parallel a$ device at 1.6 K, $R_{xx}^{2\omega}$ is zero at zero field. When the R_{xx}^{ω} gets a finite value in the vortex state above a positive external field of 0.05 T, $R_{xx}^{2\omega}$ suddenly increases and reaches the maximum negative value of -10 mΩ at around 0.13 T. As an increasing external magnetic field leads to a decreasing T_c, this behavior reflects the vortex ratchet motion by the asymmetric pinning potential, and is in accord with the previous cases of low-dimensional noncentrosymmetric superconductors.[8,23] $R_{xx}^{2\omega}$ is suppressed when further increasing the magnetic field, and it undergoes a crossover from negative to positive. The broad but small positive region of $R_{xx}^{2\omega}$ also agrees with the paraconductivity effect observed in other noncentrosymmetric superconductors.[21,22,24] At even larger magnetic field, R_{xx}^{ω} goes back to the normal state resistance and $R_{xx}^{2\omega}$ is again zero. With increasing temperature, the peak of $R_{xx}^{2\omega}$ gradually shifts towards zero field, and becomes indiscernible above T_c.

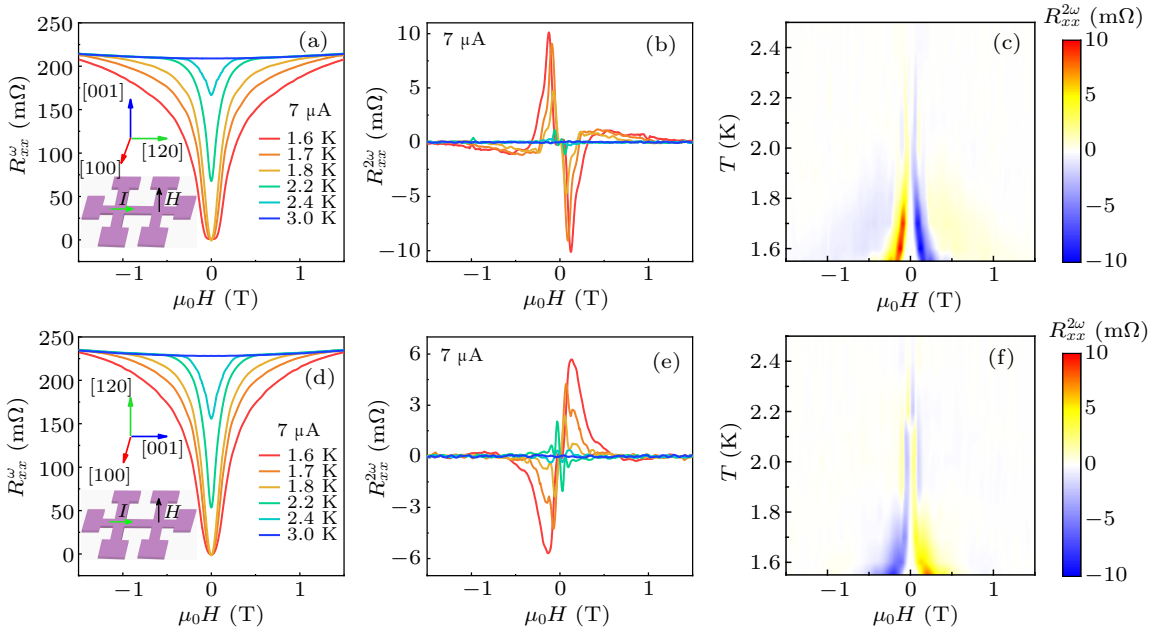


Fig. 2. (a) The first-harmonic resistance R_{xx}^{ω} and (b) the second-harmonic resistance $R_{xx}^{2\omega}$ signals of the microdevice at various temperatures under an excitation current of 7 μA along the *ab* plane. (c) Corresponding color mapping of $R_{xx}^{2\omega}$ as a function of magnetic field and temperature. (d)–(f) The same as (a)–(c) except that the current is along the *c* axis.

In addition to the field and temperature, we find that the device orientation also matters in the nonreciprocal charge transport phenomenon. Despite of the nearly identical R_{xx}^{ω} curves for the $I \parallel c$, $H \parallel a$ device, the sign of $R_{xx}^{2\omega}$ is reversed at 1.6 K, and the peaks are broader as shown in Fig. 2(e). There is another sign reversal of the overall profile above 2 K. We plot color maps showing the systematic evolution of $R_{xx}^{2\omega}$ amplitude as a function of both magnetic field and temperature in Figs. 2(c) and 2(f).

We also measure the $R_{xx}^{2\omega}$ of the microdevices at ac currents of different amplitudes. Figures 3(a) and 3(d) depict the first harmonic resistance R_{xx}^{ω} of the device with two directions measured at $T = 1.6$ K with current increasing from 2 μA to 300 μA. The overall effect of a larger current is similar to the rising of temperature, due to the current induced surface magnetization and the Joule heating on the electrodes. The larger the current is, the easier the magnetic field will bring the system into resistive states. Correspondingly, the second harmonic resistance $R_{xx}^{2\omega}$ firstly increases and then decreases as the current increases, as shown in Figs. 3(b) and 3(e). However, a change in sign occurs in nonreciprocal charge transport at high current densities (above 4.7×10^7 A/m^2), despite the relatively small signal. This indicates that nonreciprocal charge transport here may have two distinct contributions which dominate in different current or magnetic field regimes.[19,21]

Figures 4(a) and 4(b) show the maximum second harmonic resistance $R_{xx}^{2\omega}$ at the positive field as a function of temperature and electric current, respectively, which is further converted to the coefficient γ using Eq. (3) as shown in Figs. 4(c) and 4(d). The absolute $|\gamma|$ increases with decreasing temperature, and saturates at about 6×10^5 T^{-1}·A^{-1} below 2 K as shown in Fig. 4(c), which is attributed to the vortex dynamics nature of nonreciprocal charge transport.[25] This value is much larger compared with known rectification effects in the low-dimensional noncentrosymmetric superconductors like $NbSe_2$[24] and the topological kagome superconductor CsV_3Sb_5,[19] and competes with the largest one in T_d-$MoTe_2$ thin film.[34,35] It should be noted that for a better comparison among different systems, the normalized coefficient $\gamma' = A_\perp \gamma$ instead of γ is more appropriate.[15,17] Here $A_\perp$ is the sample's cross-section area along the current direction, and γ' does not

depend on the detailed sample geometry. We find that the γ' for our $NbGe_2$ devices reaches $4 \times 10^{-7} m^2 \cdot T^{-1} \cdot A^{-1}$, a value larger than that of most low-dimensional noncentrosymmetric superconductors, suggesting the potential of $NbGe_2$ to realize rectification devices with high efficiency and low energy cost. The detailed mechanism of such a large γ' deserves further studies. The current dependence of γ' in Fig. 4(d) is similar to that in Fig. 4(c), except a sign reversal around 30 μA.

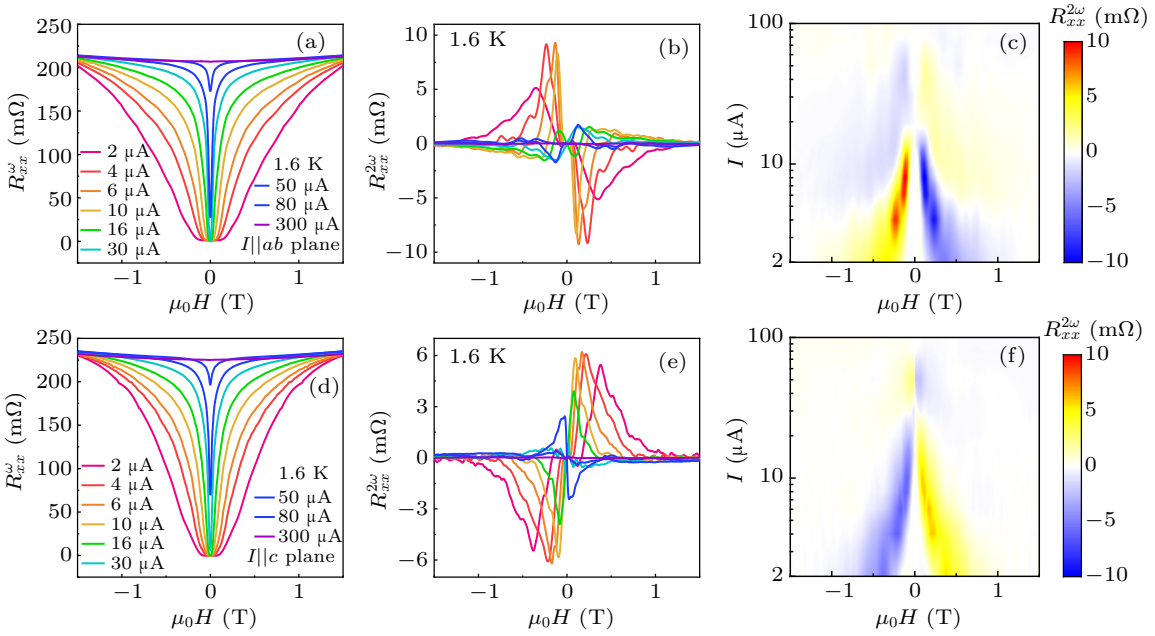


Fig. 3. (a) The first-harmonic resistance R^{ω}_{xx} and (b) the second-harmonic resistance $R^{2\omega}_{xx}$ of the microdevice at various currents along *ab* plane at 1.6 K. (c) Corresponding color mapping of the $R^{2\omega}_{xx}$ as a function of magnetic field and current. (d)–(f) The same as (a)–(c) except that the current is along the *c* axis.

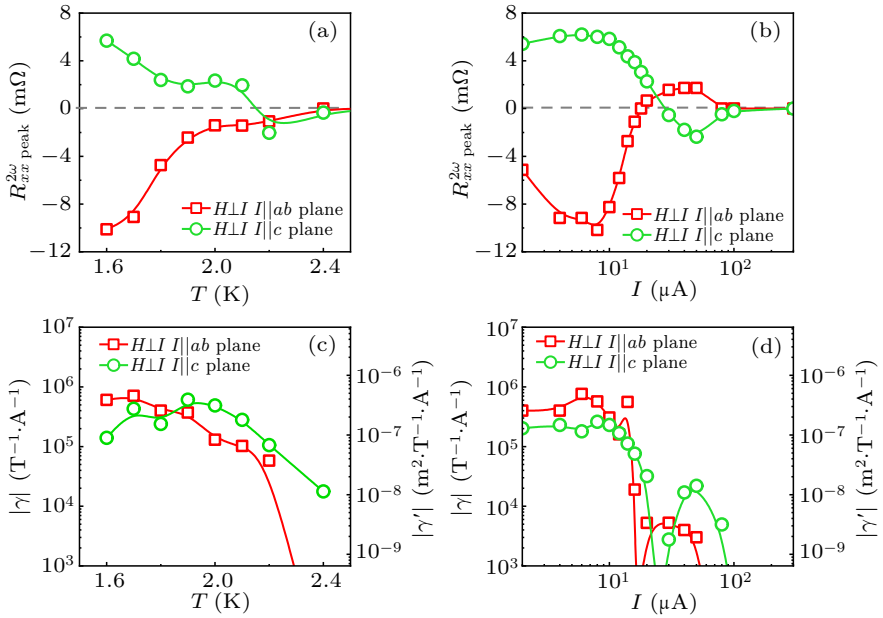


Fig. 4. (a) Amplitude of second-harmonic resistance at the peak position ($R^{2\omega}_{xx}$) as a function of the temperature in the positive field region. (b) Amplitude of $R^{2\omega}_{xx}$ at the peak position as a function of the applied current. The absolute value of the nonreciprocal coefficient $\gamma = \frac{2R^{2\omega}_{xx}}{R^{\omega}_{xx} BI}$ (left axis) and $\gamma' = A_{\perp}\gamma$ (right axis) as a function of (c) the temperature and (d) the current.

4. Conclusions

In summary, we have investigated the nonreciprocal charge transport in microdevices of the superconductor $NbGe_2$ with structural chirality. Giant superconducting rectification effect from vortex dynamics has been demonstrated during the superconducting transition, with rectification coefficient $\gamma = 6 \times 10^5\ T^{-1} \cdot A^{-1}$ being one of the largest values recorded so far. We also report the tunability of the rectification effect through the temperature, the current and the device orientation. Our results help understanding the nonreciprocal trans-

port in superconductor with structural chirality, and offer ways of manipulation on the superconducting rectification devices.

Acknowledgements

Project supported by the National Key R & D Program of China (Grant No. 2022YFA1403603), the National Natural Science Foundation of China (Grant Nos. U2032213, 12104461, 12374129, and 12304156), and Chinese Academy of Sciences (Grant Nos. YSBR-084, and JZHKYPT-2021-08). A portion of this work was supported by the High Magnetic Field Laboratory of Anhui Province.

References

[1] Wagnière G H 2007 *On chirality and the universal asymmetry: reflections on image and mirror image* (John Wiley & Sons)
[2] Chang G, Wieder B J, Schindler F, Sanchez D S, Belopolski I, Huang S M, Singh B, Wu D, Chang T R, Neupert T, Xu S Y, Lin H and Hasan M Z 2018 *Nat. Mater.* **17** 978
[3] Chang G, Xu S Y, Wieder B J, Sanchez D S, Huang S M, Belopolski I, Chang T R, Zhang S, Bansil A, Lin H and Hasan M Z 2017 *Phys. Rev. Lett.* **119** 206401
[4] Tokura Y and Nagaosa N 2018 *Nat. Commun.* **9** 3740
[5] Atzori M, Train C, Hillard E A, Avarvari N and Rikken G L J A 2021 *Chirality* **33** 844
[6] Cheong S W and Xu X 2022 *npj Quantum Mater.* **7** 40
[7] Yu T, Luo Z and Bauer G E 2023 *Phys. Rep.* **1009** 1
[8] Hoshino S, Wakatsuki R, Hamamoto K and Nagaosa N 2018 *Phys. Rev. B* **98** 054510
[9] Fasman G D 2013 *Circular dichroism and the conformational analysis of biomolecules* (Springer Science & Business Media)
[10] Bogdanov A and Hubert A 1994 *J. Magn. Magn. Mater.* **138** 255
[11] Rikken G L J A, Fölling J and Wyder P 2001 *Phys. Rev. Lett.* **87** 236602
[12] Yoda T, Yokoyama T and Murakami S 2015 *Sci. Rep.* **5** 12024
[13] Saito Y, Nakamura Y, Bahramy M S, Kohama Y, Ye J, Kasahara Y, Nakagawa Y, Onga M, Tokunaga M and Nojima T 2016 *Nat. Phys.* **12** 144
[14] Wang N, Kaplan D, Zhang Z, Holder T, Cao N, Wang A, Zhou X, Zhou F, Jiang Z and Zhang C 2023 *Nature* **621** 487
[15] Wang Y, Legg H F, Bömerich T, Park J, Biesenkamp S, Taskin A A, Braden M, Rosch A and Ando Y 2022 *Phys. Rev. Lett.* **128** 176602
[16] Ideue T, Hamamoto K, Koshikawa S, Ezawa M, Shimizu S, Kaneko Y, Tokura Y, Nagaosa N and Iwasa Y 2017 *Nat. Phys.* **13** 578
[17] Morimoto T and Nagaosa N 2016 *Phys. Rev. Lett.* **117** 146603
[18] Yoshimi R, Kawamura M, Yasuda K, Tsukazaki A, Takahashi K S, Kawasaki M and Tokura Y 2022 *Phys. Rev. B* **106** 115202
[19] Wu Y, Wang Q, Zhou X, Wang J, Dong P, He J, Ding Y, Teng B, Zhang Y, Li Y, Zhao C, Zhang H, Liu J, Qi Y, Watanabe K, Taniguchi T and Li J 2022 *npj Quantum Mater.* **7** 105
[20] Daido A, Ikeda Y and Yanase Y 2022 *Phys. Rev. Lett.* **128** 037001
[21] Wakatsuki R, Saito Y, Hoshino S, Itahashi Y M, Ideue T, Ezawa M, Iwasa Y and Nagaosa N 2017 *Sci. Adv.* **3** e1602390
[22] Itahashi Y M, Ideue T, Saito Y, Shimizu S, Ouchi T, Nojima T and Iwasa Y 2020 *Sci. Adv.* **6** eaay9120
[23] Itahashi Y M, Saito Y, Ideue T, Nojima T and Iwasa Y 2020 *Phys. Rev. Res.* **2** 023127
[24] Zhang E, Xu X, Zou Y C, Ai L, Dong X, Huang C, Leng P, Liu S, Zhang Y, Jia Z, Peng X, Zhao M, Yang Y, Li Z, Guo H, Haigh S J, Nagaosa N, Shen J and Xiu F 2020 *Nat. Commun.* **11** 5634
[25] Ideue T, Koshikawa S, Namiki H, Sasagawa T and Iwasa Y 2020 *Phys. Rev. Res.* **2** 042046
[26] Wakatsuki R and Nagaosa N 2018 *Phys. Rev. Lett.* **121** 026601
[27] Remeika J P, Cooper A S, Fisk Z and Johnston D C 1978 *J. Less-Common Met.* **62** 211
[28] Lv B, Li M, Chen J, Yang Y, Wu S, Qiao L, Guan F, Xing H, Tao Q, Cao G H and Xu Z A 2020 *Phys. Rev. B* **102** 064507
[29] Yang H Y, Yao X, Plisson V, Mozaffari S, Scheifers J P, Savvidou A F, Choi E S, McCandless G T, Padlewski M F, Putzke C, Moll P J W, Chan J Y, Balicas L, Burch K S and Tafti F 2021 *Nat. Commun.* **12** 5292
[30] Sato Y J, Nakamura A, Nishinakayama R, Okazaki R, Harima H and Aoki D 2023 *Phys. Rev. B* **108** 235115
[31] Pop F, Auban-Senzier P, Canadell E, Rikken G L J A and Avarvari N 2014 *Nat. Commun.* **5** 3757
[32] Rikken G L J A and Wyder P 2005 *Phys. Rev. Lett.* **94** 016601
[33] Emmanouilidou E, Mardanya S, Xing J, Reddy P V S, Agarwal A, Chang T R and Ni N 2020 *Phys. Rev. B* **102** 235144
[34] Du W S, Chen W, Zhou Y, Zhou T, Liu G, Zhang Z, Miao Z, Jia H, Liu S and Zhao Y 2023 arXiv: 2303.09052
[35] Wakamura T, Hashisaka M, Hoshino S, Bard M, Okazaki S, Sasagawa T, Taniguchi T, Watanabe K, Muraki K and Kumada N 2024 *Phys. Rev. Res.* **6** 013132